

Article

Testing the Physical and Mechanical Properties of Polyacrylonitrile Nanofibers Reinforced with Succinite and Silicon Dioxide Nanoparticles

Inga Lasenko ^{1,*}, Dace Grauda ², Dalius Butkauskas ³, Jaymin Vrajlal Sanchaniya ^{1,4}, Arta Viluma-Gudmona ^{1,4} and Vitalijs Lusis ⁵

- ¹ Mechanics and Biotextile Research Laboratory, Riga Technical University, 3/3-20 Pulka Street, LV-1007 Riga, Latvia; jaymin.sanchaniya@rtu.lv (J.V.S.); arta.viluma.gudmona@rtu.lv (A.V.-G.)
- ² Institute of Biology, University of Latvia, 19 Raina Blvd, LV-1586 Riga, Latvia; dace.grauda@lu.lv
- ³ Scientific Research Institute Nature Research Centre (NRC), 2 Akademijos Street, LT08412 Vilnius, Lithuania; dalius.butkauskas@gamtc.lt
- ⁴ Department of Theoretical Mechanics and Strength of Materials, Riga Technical University, 6B Kipsalas Street, LV-1048 Riga, Latvia
- ⁵ Research Centre for Ecological Construction, Faculty of Civil Engineering, Riga Technical University, 1 Paula Valdena Street, LV-1048 Riga, Latvia; vitalijs.lusis@rtu.lv
- * Correspondence: inga.lasenko@rtu.lv

Abstract: In this research, we focused on testing the physical and mechanical properties of the developed polyacrylonitrile (PAN) composite nanofibers with succinite (Baltic amber) and SiO₂ particles using standard methods of nanofiber testing (physical and mechanical properties). Polyacrylonitrile composite nanofibers (based on the electrospinning method) were coated on an aluminum substrate for structural investigation. SEM was used to determine the average fiber diameter and standard deviation. The mechanical properties of the fibers were determined using a universal testing machine (NANO, MTS). We observed that constant or decreased levels of crystallinity in the ultrafine composite nanofibers led to the preservation of high levels of strain at failure and that the strength of nanofibers increased substantially as their diameter reduced. Improvements in PAN composite nanofibers with succinite and SiO₂ nanopowder are feasible with continuous decreases in diameter. The drastically decreased strain at failure demonstrated a substantial reduction in viscosity (toughness) of the annealed nanofibers. Large stresses at failure in the as-spun nanofibers were a result of their low crystallinity. As a result, decreasing the diameter of PAN nanofibers from approximately 2 micrometers to 139 nanometers (the smallest nanofiber tested) resulted in instantaneous increases in the elastic modulus from 1 to 26 GPa, true strength from 100 to 1750 MPa, and toughness from 20 to 604 MPa.

Keywords: succinite and SiO₂ nanoparticles; strength of nanofibers; nanofiber composite



Citation: Lasenko, I.; Grauda, D.; Butkauskas, D.; Sanchaniya, J.V.; Viluma-Gudmona, A.; Lusis, V. Testing the Physical and Mechanical Properties of Polyacrylonitrile Nanofibers Reinforced with Succinite and Silicon Dioxide Nanoparticles. *Textiles* **2022**, *2*, 162–173. <https://doi.org/10.3390/textiles2010009>

Academic Editor: Issei Otsuka

Received: 9 November 2021

Accepted: 28 February 2022

Published: 8 March 2022

Publisher's Note: MDPI stays neutral with regard to jurisdictional claims in published maps and institutional affiliations.



Copyright: © 2022 by the authors. Licensee MDPI, Basel, Switzerland. This article is an open access article distributed under the terms and conditions of the Creative Commons Attribution (CC BY) license (<https://creativecommons.org/licenses/by/4.0/>).

1. Introduction

In the past, one of the main engineering challenges was the development, introduction, and mass production of efficient materials in all industrial areas. Different fiber-reinforcement options are used in various fields [1–5], including the use of various materials and technologies [6–9]. Due to its superior physical characteristics, such as low density, thermal constancy, high strength, and modulus of elasticity, polyacrylonitrile (PAN) is a commercially important semicrystalline polymer [10,11]. The fabrication of PAN composites, also known as polymer nanocomposites (PNCs), is a relatively new area of study that has the potential to considerably enhance the mechanical characteristics of PAN. PAN, a typical material for electrospinning, is carbonized with various organic nanoparticles. Alternatively, inorganic components, such as MgO or ZnO, may be included [12].

PAN is often used in a two-step procedure to create carbon nanofibers. In particular, nanographite-filled polymers can be used to create conductive areas on textile fabrics. Most commonly, polyurethane is used for this purpose. Graphite-filled polyacrylonitrile has the advantage of not requiring toxic precursors, which is not true of polyurethane. Generally, such PAN/graphite coatings can be applied to textile fabrics. Additionally, PAN is one of the few nontoxic, solvent-spun, water-resistant polymers [13]. In general, nanofillers, such as nanoclays (layered silicates), are characterized as having at least one dimension in the range of 1–100 nm. Due to their nanoscale size, high specific surface area, and related preponderance of interfaces, trace quantities of nanofillers (usually 1–4 vol %) are capable of substantially altering the structure and morphology of PNCs at the molecular level [14,15]. This implies that they can influence material characteristics at a scale at which conventional micron-sized fillers cannot. The resultant PNCs have property profiles that are suitable for a broad variety of industrial applications, including high stiffness, chemical and heat resistance, dimensional stability, decreased water absorption, and enhanced electric and optical characteristics [16,17]. The purpose of nanofillers in structural applications is to improve the stiffness of the polymer matrix while increasing the toughness through novel energy-dissipation processes [18,19]. As a result, developing PNCs with an optimal balance of characteristics requires a high degree of connection between processing and morphological and micromechanical control. Nanofillers often agglomerate inside the polymer matrix. Due to their high agglomeration propensity, their capacity to bind with the matrix is substantially reduced, lowering the effective aspect ratio of the reinforcement. Furthermore, when an external load is applied, stresses easily concentrate around such agglomerates, resulting in the system failing prematurely. Electrospinning has been used as a substitute method to combat the agglomeration propensity of nanofillers [20–22]. Electrospinning results in a homogenous dispersion of nanofillers, such as layered silicates, carbon nanotubes, and many others, inside the fibers, as well as a dramatic reduction in the fiber diameter to several tens of nanometers. The resultant nanofibers are continuous and therefore have a high aspect ratio, as well as a high specific surface area, which strongly interacts with the environment, especially exposure to ultraviolet radiation.

In the scientific literature, no approach has been applied to combine succinite and silicon oxide nanoparticles with PAN to prepare an ultraviolet (UV)-resistant and protective material. Polyacrylonitrile fibers are UV-resistant [23]. Succinite particles (0.8–3 μm) were able to defend against UV-C in a 100–280 nm area [24], and silicon oxide particles (200–400 nm) were able to defend against UV-B in a 280–315 nm area [25].

In this research, we tested the physical and mechanical properties of the resulting PAN nanofibers with succinate and silicon oxide nanoparticles.

2. Materials and Methods

2.1. Materials and Fiber Fabrication

Succinite and silicon dioxide nanoparticles were used to prepare PAN composite nanofibers. Succinite (Baltic amber) powder (JLU Technologies Ltd., Riga, Latvia (LV1082); CAS: 9000-02-6) of 105–188 μm was ground to a particle size of 5 ± 1 nm. SiO_2 nanoparticles (Sigma-Aldrich chemicals, Merck KGaA, Darmstadt, (64287) Germany; CAS Number: 7631-86-9) of 5 ± 0.5 nm were employed in the solution by stirring at ambient conditions for 2 h (room temperature = 22 ± 1 °C; moisture content, 60%). The solvent was used for the production of PAN composite nanofibers from 16–20 wt % solution of the PAN polymer at ambient conditions (Pfaltz and Bauer, Inc., Waterbury, (CT06708), USA; cat# P21470, MW 150,000) in dimethylformamide (DMF) (Sigma-Aldrich, Merck KGaA, Darmstadt, (64287) Germany; cat# 271012). Then, the suspension was maintained in a Branson 1800 Series ultrasonic bath (Fisher Scientific Company, LLC; Cpx1800h Digital Ultrasonic Bath, Danbury, (CT06811), USA) for 5 h to grind microparticles into a nanostructure. PAN nanofibers containing 3% wt/wt succinite and 1% wt/wt SiO_2 nanoparticles were electrospun (Fisherbrand™ Single Syringe Pump, a needle-based electrospinning machine, Danbury, (CT06811), USA) with a spinning-chamber temperature of 22 ± 1 °C and 36%

relative humidity using a 20 Ga needle from the 16–20 wt % solution of the polymer. The PAN composite nanofibers were gathered on a stationary collector. The applied voltage was 10,000 to 12,000 volts, with a resulting current of ~ 0.1 mA, a carriage speed of 110 mm/s, and a distance between the spinneret needle (electrospinning device) and target (covered by aluminum foil; thickness, 35 μm ; Vireo.de, Merseburg, (06217) Germany) of 20 cm. The diameters of the fibers were changed by changing the voltage and PAN concentration. Similar electrospinning settings were used to produce as-spun and annealed fibers. Annealing was carried out for 1 h at 130 and 180 $^{\circ}\text{C}$ in air in order to avoid overoxidation, with a heating rate of up to 5 $^{\circ}\text{C}/\text{min}^2$ (forced-air oven, SKU F019140, Cornelius, (OR97113), USA).

2.2. Preparation of Specimens and Mechanical Testing

The mechanical properties of individual PAN composite nanofibers were determined using a universal testing machine (NANO) at a constant strain rate of 0.005 s^{-1} . Electrospun PAN composite nanofibers with a length of 3 ± 1 cm were created using a split electrode. A wire fork was used to pick up individual fibers. A 7 ± 4 mm piece of the PAN composite nanofiber (the gauge length used in this research) was bonded to special carton grips using an epoxy adhesive and transferred for mechanical testing on a universal testing machine (NANO, New York, (NY10027), USA). A segment of adjacent nanofiber was investigated to determine its morphology and diameter with a Hitachi High-Tech TM Series TM3030 Plus scanning electron microscope (The Netherlands) using ImageJ software (software version 1.53e, 2021, National Institutes of Health, Bethesda, MD, USA). To determine its mechanical characteristics, the diameter was measured in at least three spots along the body of the nanofiber. This measurement was required in order to calculate the diameter of nanofiber distribution by number and volume. As-spun fibers were elastoplastic, exhibiting significant deformations until failure. We converted measured load and displacement fluctuations to engineering and real stresses and strains; the resulting stress–strain graphs are presented in subchapter Results. True stress and strain are often employed to explain the behavior of composite polymer materials when subjected to significant deformations. From the resulting stress–strain diagrams, the modulus, strain at failure, failure stress (strength), and toughness (area under the curve) of the PAN nanofiber were determined. Modulus and toughness were calculated using stress–strain diagrams from engineering stress. A total of 152 tests were performed on the as-spun nanofibers, and 124 and 150 tests were performed on the nanofibers annealed at 130 and 180 $^{\circ}\text{C}$, respectively. In total, 426 tests were performed on the nanofibers.

2.3. Structural Investigation

PAN composite nanofiber mats were electrospun on an aluminum substrate for structural investigation. Optical images of the PAN composite nanofiber mats, including those annealed at 130 and 180 $^{\circ}\text{C}$, are shown in Figure 1. SEM was used to determine the average diameter of the PAN composite nanofibers as well as standard deviation. At least 200 PAN composite nanofibers from multiple locations were evaluated for each examined sample. A wide-angle X-ray diffraction study of the PAN composite nanofibers was carried out using a Rigaku Multiflex X-ray diffractometer with Cu $K\alpha$ radiation and a wavelength between 10 and 50 degrees. After removing the background, the crystalline peak (or peaks in the case of annealed samples), and amorphous halo were fitted using Lorentzian peak morphologies, as shown in Figure 2. For each nanofiber family, at least three samples with varying average nanofiber sizes were examined (i.e., as-spun nanofibers and nanofibers annealed at 130 and 180 $^{\circ}\text{C}$; optical images are shown in Figure 1).

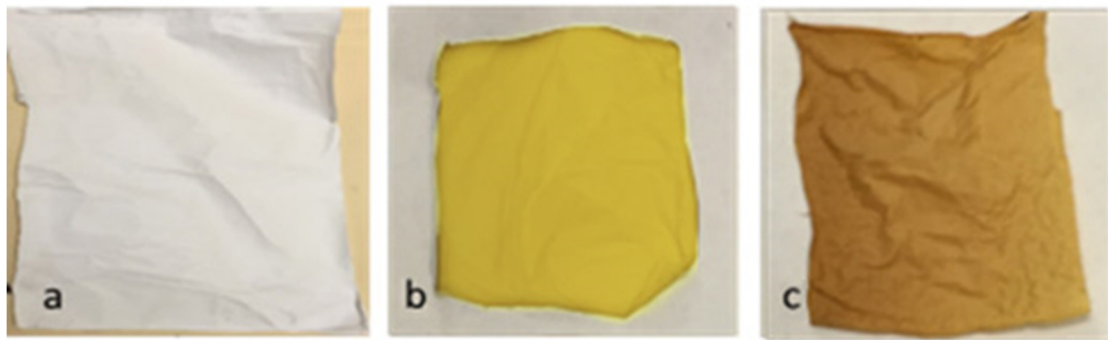


Figure 1. Optical images of 16% electrospun PAN composite nanofiber mat heated to different temperatures in air: (a) as spun; (b) annealed at 130 °C for 1 h; (c) annealed at 180 °C for 1 h.

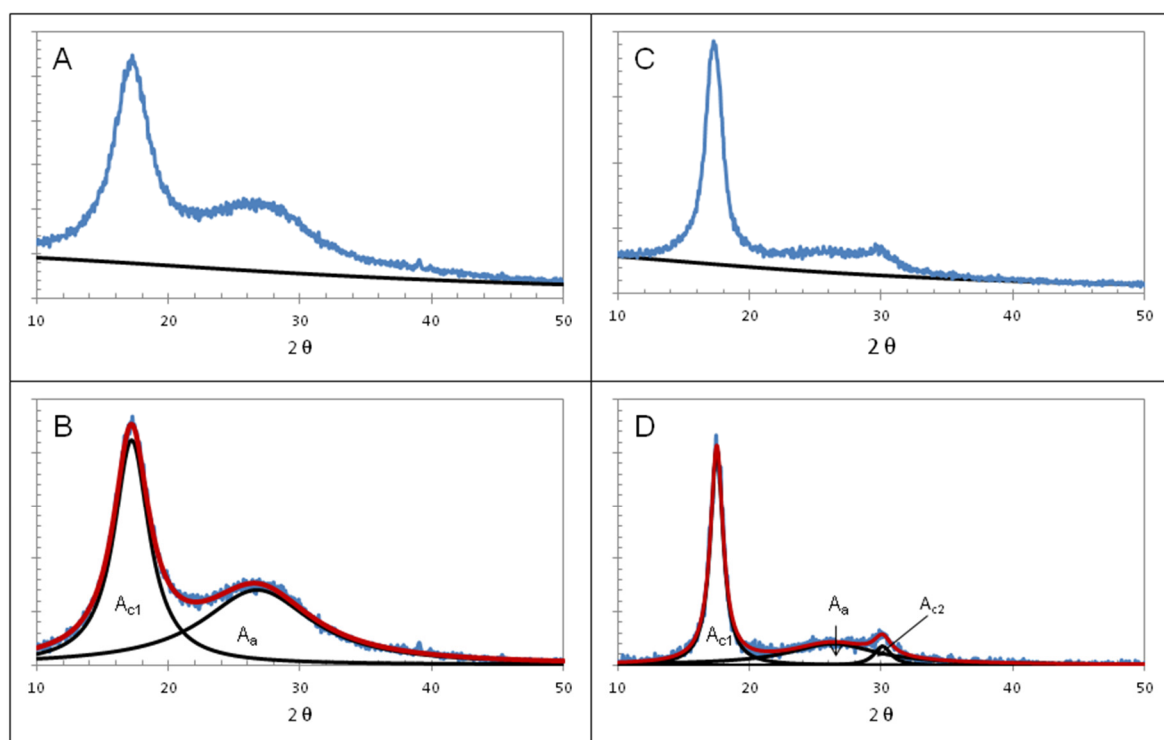


Figure 2. Schematic illustrating XRD spectra analysis for (A,B) as-spun and (C,D) annealed composite nanofiber specimens.

The color of the nanofiber mat darkened with increasing temperature as a result of the different mixtures of the structures produced during stabilization. In industrial applications, changes in color are used as a qualitative indicator of the progression of the stabilization process [26].

The XRD spectra of composite nanofibers annealed at 130 and 180 °C were qualitatively comparable.

The crystallinity of the XRD patterns was determined by dividing the area under the crystalline peaks by the total area beneath the curve as follows:

$$\% \text{crystallinity} = \frac{A_{c1} + A_{c2}}{A_{c1} + A_{c2} + A_{c3}} \cdot 100 \quad (1)$$

The coherence length from the width of the primary crystalline peak was estimated using the Scherer equation as follows:

$$C.L. (\text{\AA}) = \frac{K\lambda}{\beta \cos\theta} = \frac{0.9 \cdot 1.542}{\sqrt{(FWHM(\text{Rad})^2 - 0.002^2)} \cos\theta} \quad (2)$$

where the form factor was set to 0.9, the wavelength λ (standard) for a copper (Cu) source was 0.002, the instrumental peak widening was estimated using a single-crystal Si standard, and the Bragg angle for the crystalline peak was $2\theta \sim 17^\circ$.

3. Results

The stress–strain graphs of typical as-spun composite nanofibers with various diameters are illustrated in Figure 3E. As the nanofiber diameter decreased, modulus and ultimate strength increased, whereas strain at failure remained relatively unaffected by the diameter.

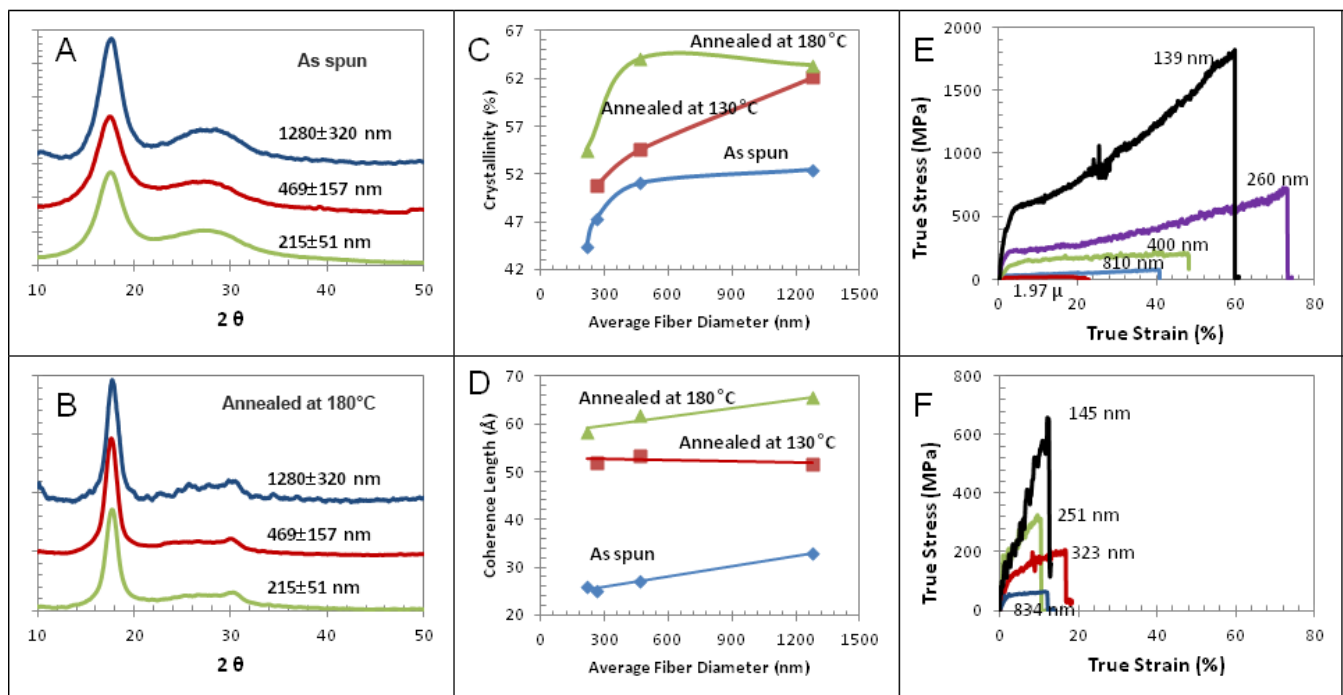


Figure 3. Effects of PAN composite nanofiber (with succinite and SiO₂ nanopowder) diameter and annealing on crystallinity and mechanical behavior. Wide-angle X-ray diffractograms for (A) as-spun and (B) annealed composite nanofiber mats with different average fiber diameters (XRD spectra for composite nanofibers annealed at 130 and 180 °C were qualitatively similar); variations in (C) XRD crystallinity and (D) coherence length as functions of average fiber diameter; representative stress–strain diagrams for (E) individual as-spun and (F) annealed PAN composite nanofibers (with succinite and SiO₂ nanopowder) of different diameters. The same strain scale is used in panels (E,F) for easier comparison and evaluation of annealing effects.

The experimental scatter in mechanical studies of individual composite nanofibers reported to date has been quite high. This is typical in fiber research and is particularly true in the case of experimental fibers. The number of individual fiber specimens tested in this study (sample size) is the largest reported to date. Despite large experimental scatter, particularly for strain at failure (the most defect-sensitive experimental parameter in this study), the trends of increasing modulus and strength, as well as relative insensitivity of strain at failure, with decreasing composite nanofiber diameter are clearly visible in Figure 2A–C. These trends led to a remarkable increase in toughness, as shown in Figure 2D.

The observed improvements in elastic modulus and, to a lesser extent, strength may be ascribed to the improved macromolecular orientation of nanofibers; other mechanisms may also affect strength, such as reduced concentration, size of defects, and increased defect insensitivity with confinement. Extensive evidence of macromolecular orientation in electrospun PAN composite nanofibers has been reported [27–31]. The majority of researchers used bunches of nanofibers with large diameters (thousands of nanometers). Alignment further decreases diameter to the sub-200 nm range, which has shown the highest performance in this and other mechanical studies.

An enhanced macromolecular orientation, usually obtained via drawing, leads to increased crystallinity in traditional polymer fibers and films. Drawing PAN sheets was found to cause the amorphous halo to vanish in XRD diffractograms [32]; the XRD spectra of PAN material and undrawn cast film closely resembled the spectra obtained in the current study (Figure 2A,B). X-ray analysis of PAN composite nanofibers (with succinite and SiO₂ nanopowder) with different diameters demonstrated that the crystallinity of as-spun nanofibers did not increase with decreasing nanofiber diameter but was reduced, resulting in finer diameters (Figure 3C). Others reported low crystallinity in electrospun nanofibers, often ascribed to rapid solvent evaporation from electrospun jets, resulting in quick jet solidification. PAN/DMF jets were recently subjected to theoretical study [33], which confirmed ultrafast solvent evaporation from sub-micrometer jets, supporting the possible link between solvent evaporation and low crystallinity. Another possible mechanism is a high concentration of polymer macromolecules located near the fiber surface. Although most surface and confinement effects reported for polymer films were not observed in films thicker than 30–40 nanometers, the effects may be more severe in nanofibers due to the two-dimensional nature of their confinement. Thus, we hypothesized that constant or reduced levels of crystallinity in ultrafine nanofibers lead to the preservation of high levels of strain at failure when nanofiber strength increases significantly with decreasing diameter.

Individual nanofibers are difficult to analyze due to the low sensitivity of most analytical techniques, as well as polymer radiation damage. TEM analysis of the ultrafine nanofibers failed to show any crystallinity. This result is similar to that of an HRTEM analysis of PAN nanofibers performed in [34]. Crystallinity was also lacking in as-electrospun nanofibers analyzed by a synchrotron wide-angle X-ray diffractometer at room temperature [35]. These results do not necessarily contradict those of the XRD analysis in the present study. XRD analysis was carried out on PAN composite nanofibers with wide diameter distributions, as shown in Figure 3 (panel A). We found a substantial decrease in the average crystallinity of as-spun nanofibers with decreasing average diameter of the nanofibers (Figure 3C). As the mat findings are dominated by the largest fibers in the existing sample, the crystallinity of the smallest PAN composite nanofibers may be considerably lower than the average value obtained for nanofiber mats. To further elucidate the role of crystallinity in the mechanical properties of composite nanofibers, we attempted to change crystallinity by annealing. Annealing is often used to improve crystallinity and attain the perfection of quickly solidified polymers. Two annealing temperatures were chosen to investigate the range between the glass transition temperature of polyacrylonitrile (90–120 °C) and the oxidation temperature. In [34], a considerable increase in the rate of crystal formation above 100 °C was observed for PAN nanofibers produced from a polymer with a molecular weight comparable to that used in our research. Polyacrylonitrile oxidation, a critical step in the conversion of polyacrylonitrile precursors to carbon, is typically carried out between 200 and 300 °C. The two annealing temperatures selected were 130 and 180 °C. Wide-angle X-ray examination of the annealed composite nanofibers verified the rises in crystallinity and crystal size throughout the range of diameters of the composite nanofiber (Figure 3B–D). Similar to unspun composite nanofibers, the degree of crystallinity of annealed samples dropped as the average diameter decreased. This may have occurred because of the initial structure of nanofibers with varying diameters (see data for as-spun nanofibers with varying diameters) or to the ongoing confinement effect.

Mechanical tests of individual annealed composite nanofibers revealed a substantial increase in nanofiber modulus, compared with that in as-spun nanofibers of comparable sizes. Strength values were comparable or slightly higher. However, the failure strain of composite nanofibers substantially decreased. The stresses at failure, shown in Figures 2C and 3F, were within the range of strains seen in commercial polymer fibers, such as polyester, polyamide 6, nylon 66, and Nomex. Annealed PAN nanofibers (with succinite and SiO₂ nanoparticles) retained a significant size effect in modulus but a somewhat lesser effect in strength. The highest recorded strength values of annealed PAN nanofibers were below the highest values for as-spun nanofibers. However, the smallest diameters of annealed composite nanofibers in the current study were slightly larger than those of the finest as-spun nanofibers, so further improvements are possible with further reduced diameter. The sharply reduced strain at failure led to a significant drop in the toughness of annealed composite nanofibers (Figure 2D). This corresponds with the enhanced crystallinity found in these nanofibers and offers further evidence of our theory that high stresses at failure occur in as-spun nanofibers as a result of their low crystallinity.

We investigated whether a correlation exists between strength and toughness as the diameter of composite nanofibers decreases. The respective parameters from the same tests are plotted in Figure 4 for each of the tested nanofiber families (multiple data points overlap in these graphs, particularly for the as-spun composite nanofibers in panel A; all tested specimens are represented in this figure). A strong, nearly linear correlation was observed for as-spun composite nanofibers (panel A). A weaker correlation was sometimes present for annealed composite nanofibers (panels B and C), albeit with a much higher slope (higher strength values at lower toughness), as shown in Figure 5, in which the data are combined for easier comparison.

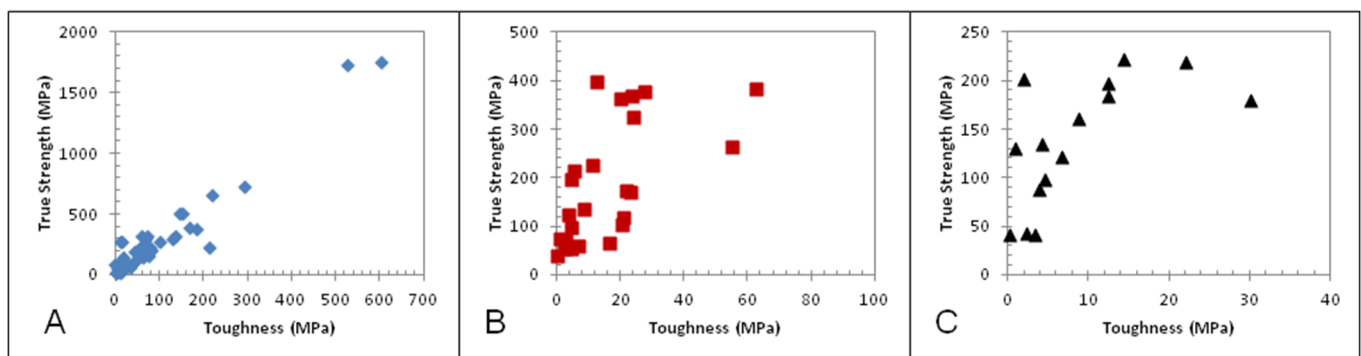


Figure 4. Correlation of strength and toughness for (A) as-spun PAN composite nanofibers (with succinite and SiO₂ nanopowder) and composite nanofibers annealed at (B) 130 °C and (C) 180 °C.

Correlations may be explained in terms of normal material behavior. The majority of structural materials have a trade-off between strength and toughness, which means that high strength is often obtained at the expense of low toughness and vice versa (Figure 5, gray area). The majority of processing methods that increase the strength of initially ductile materials, such as metals or semicrystalline polymers, cause material characteristics to shift from the bottom-right to the top-left corner of the figure.

This is true for both established techniques, such as drawing polymers and metals, and for novel ones, such as metal nanostructuring. Additionally, high-performance fibers follow this pattern, demonstrating high tensile strength and low viscosity (toughness) (Figure 2, panel D). The goal is to reach the top-right corner of the figure for safety-critical applications requiring both high strength and fracture resistance. The proven ability of electrospun nanofibers to move toward the top-right corner as their diameter decreases is unique and promising.

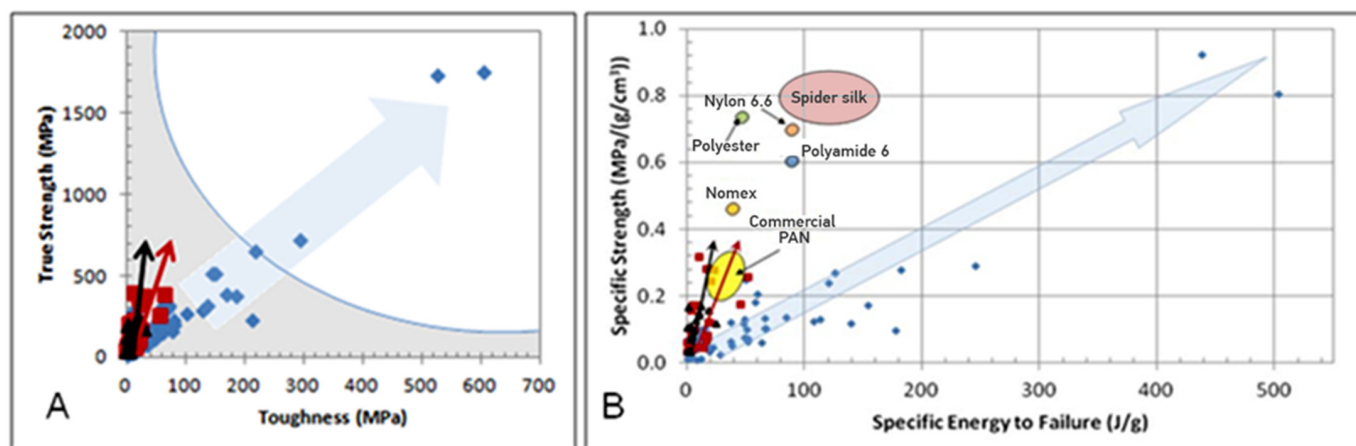


Figure 5. Correlations of normal materials behavior, the structural materials have a trade-off between strength and toughness; (A) correlation between toughness and strength compared to as-spun PAN composite nanofibers and annealed composite nanofibers, high strength is often obtained at the expense of low toughness and vice versa, gray area; (B) comparison of the strength and energy required for failure of PAN composite nanofibers used in this research (test report) with selected materials [36].

4. Discussion

The strength of the majority of fibrous materials increases as their diameter decreases. The discovery of the diameter-dependent strength of glass fibers prompted the invention of modern fracture. However, these gains in strength are often modest, and toughness normally does not increase but can decrease, as in the case of polymer fibers. In this study, decreasing the diameter of PAN composite nanofibers (containing succinite and SiO₂ nanoparticles) from approximately 2 micrometers to 139 nanometers (the smallest nanofiber tested) resulted in simultaneous increases in elastic modulus from 1 to 26 GPa, true strength from 100 to 750 MPa, and toughness from 20 to 604 MPa. Preferred nanofibers exhibit properties that far exceed those of commercial PAN fibers and outperform, in terms of strength and modulus, the majority of commercial polymer textile fibers [37], exhibiting a 6–10-fold increase in toughness. The highest strength ever reported for PAN nanofibers is comparable to that ever documented for silk fiber [28,38,39], with three times higher toughness. Finally, the most favorable properties of as-spun PAN composite nanofiber compare favorably with those of most novel carbon nanotube (CNT) fibers currently under development (thinnest yarn properties, approaching the highest published values of CNT fiber toughness) [36,40–44]. Although annealed composite nanofibers have lower toughness than as-spun PAN composite nanofibers, their strain at failure does not seem to diminish with reduced diameter, resulting in a steeper but still positive connection between toughness and strength (Figure 5). As a consequence, altering the crystallinity of nanofibers through annealing or other techniques may be used to modify and finetune nanofiber characteristics and expand the coverage of material design space. We emphasize that the observed reduction in the material of polymer crystallinity with decreased PAN nanofiber diameter may not be universal. The crystallization process of polymer materials is complicated and highly dependent on macromolecular structure, the solvent used, and a variety of other factors.

Peculiarities of crystallization during electrospinning are yet to be studied. Jung and Sodano [38] and summary in Table 1 reported increases in crystallinity of the polymer material as the diameter decreased. Low or decreasing strain to failure was also reported in this study.

Table 1. Reported size effects in individual electrospun polymer nanofibers.

Polymer	Diameter Range, nm	Property Change with Diameter Decrease			Structure	
		Modulus (E)	Strength (σ)	Failure Strain (ϵ)	Orientation	Crystallinity
PLLA [45]	270–420	Increased slightly	-	-	-	-
PCL [46]	250–1300	Increased significantly for diameters <500 nm	Increased significantly for diameters <500 nm	Size effect not reported, but failure strain decreased with increasing crystallinity	Increased significantly with diameter decrease	Increased from 50–56% (XRD) with average diameter decrease
PCL [47]	350–2500	Increased slightly, faster for diameters <700 nm	Increased slightly, faster for diameters <700 nm	Limited data, but failure strain reported to decrease for diameters <700 nm	Increased with diameter decrease	Increased gradually from 42–50% (XRD) with average diameter decrease
Nylon 6,6 [48]	400–900	Increased significantly for diameters <600 nm	-	-	Increased gradually with average diameter decrease	Increased gradually from 35–47% (XRD) with average diameter decrease
PA6(3)T [49]	170–3500	Increased for diameters <500 nm	Yield strength increased for diameters <1000 nm	Decreased significantly with decrease in diameter (based on reported stress–strain diagrams)	Increased significantly with average diameter decrease <1000 nm (polarized FTIR)	Amorphous
PCL [50] and PCLEEP	200/300–5000	Increased considerably for diameters <700 nm	Increased dramatically for diameters <700 nm	Large strains to failure; unaffected by diameter	-	No measurable change in XRD crystallinity (bundles)
PA MPS [51]	55–250	Increased significantly; faster for diameters <70 nm	-	-	-	-
PAN [52]	200–700	Increased significantly, especially for longer spinning distance (increased crystallinity, orientation)	Yield strength increased significantly	Very large ultimate strain reported to depend weakly on fiber diameter; stress–strain diagram for a 250 nm fiber exhibited 150% strain	Increased significantly with increase in spinning distance (decrease in average diameter)	Low overall crystallinity, increased slightly with increase in spinning distance (decrease in average diameter)
PAN [53]	140–3000	Increased considerably for diameters <500 nm	Increased dramatically for diameters <500 nm	-	-	-

The nanofiber diameter threshold at which nanofibers show a substantial increase in mechanical characteristics (~500 nm) corresponds to the maximum diameter of natural filaments, such as collagen fibrils (50–500 nm). Natural polymer fibers are widespread in biological organs, materials, and tissues, to which their higher toughness is often attributed [54].

5. Conclusions

Improvements in PAN composite nanofibers (with succinite and SiO₂ nanopowder) are possible with further reduced diameter. A sharply reduced strain at failure led to a significant reduction in the toughness of annealed composite nanofibers. The high failure stresses in as-spun PAN composite nanofibers are a result of their low crystallinity. In this research, decreasing the diameter of PAN composite nanofibers from about 2 micrometers to 139 nanometers (the smallest nanofiber tested) resulted in simultaneous increases in elastic modulus from 1 to 26 GPa, actual strength from 100 to 1750 MPa, and toughness from 20 to 604 MPa. Nanofibers with the most favorable characteristics reported outperform both commercial PAN fibers in terms of strength and modulus as well as the majority of commercial polymer textile fibers (as mentioned above in the Discussion Section) in terms of toughness by a factor of 6–10. The highest recorded strength of PAN composite nanofibers is comparable to that of silk fiber, with three times higher viscosity (toughness). The most favorable properties of as-spun PAN composite nanofiber compare favorably with those of most novel carbon nanotube (CNT) fibers currently under development and

are close to the highest published values of CNT fiber toughness. The diameter of PAN composite nanofibers (with succinite and SiO₂ nanopowder) is in the 200 nm range, which showed the highest performance in our mechanical studies.

Author Contributions: Conceptualization, I.L., A.V.-G., J.V.S. and D.G.; methodology, I.L., D.G., J.V.S. and D.B.; validation, I.L., A.V.-G., J.V.S. and V.L.; formal analysis, I.L., A.V.-G., J.V.S. and D.B.; investigation, I.L., A.V.-G. and J.V.S.; resources, I.L. and J.V.S.; original draft preparation, I.L., J.V.S. and A.V.-G.; review and editing, I.L., D.G. and V.L.; supervision, I.L.; funding acquisition, I.L. and J.V.S. All authors have read and agreed to the published version of the manuscript.

Funding: The funder EUREKA program (Brussels, EU), funding number Nm.ES RTD/2018/11, 14.06.2018., as well the funder Riga Technical University's (Riga, Latvia) Doctoral Grant program, funding number no. 2-00861, 2020-2023.

Data Availability Statement: All data are provided in the paper.

Acknowledgments: This research was supported by the EUREKA program (Brussels, EU), project E!11170, IFSITEX (Nm.ES RTD/2018/11, 14.06.2018.), and Riga Technical University's (Riga, Latvia) Doctoral Grant program, project no. 2-00861 (2020-2023).

Conflicts of Interest: The authors declare no conflict of interest.

References

- Benaoum, F.; Khelil, F.; Benhamena, A. Numerical analysis of reinforced concrete beams pre cracked reinforced by composite materials. *Frat. Integrità Strutt.* **2020**, *14*, 282–296. [\[CrossRef\]](#)
- Lusis, V.; Kononova, O.; Macanovskis, A.; Stonys, R.; Lasenko, I.; Krasnikovs, A. Experimental Investigation and Modelling of the Layered Concrete with Different Concentration of Short Fibers in the Layers. *Fibers* **2021**, *9*, 76. [\[CrossRef\]](#)
- Macanovskis, A.; Lukasenoks, A.; Krasnikovs, A.; Stonys, R.; Lusis, V. Composite Fibers in Concretes with Various Strengths. *ACI Mater. J.* **2018**, *115*, 647–652. [\[CrossRef\]](#)
- Bleive, L.L.; Lusis, V. Experimental study and numerical modelling for flexural capacity of FRC structural elements. *Environ. Technol. Resour. Proc. Int. Sci. Pract. Conf.* **2021**, *3*, 30–35. [\[CrossRef\]](#)
- Lusis, V.; Krasnikovs, A. Fiberconcrete with Non-Homogeneous Fibers Distribution. *Environ. Technol. Resour. Proc. Int. Sci. Pract. Conf.* **2013**, *2*, 67. [\[CrossRef\]](#)
- Duy, N.P.; Anh, V.N.; Hiep, D.V.; Anh, N.M.T. Strength of concrete columns reinforced with Glass fiber reinforced polymer. *Mag. Civ. Eng.* **2021**, *101*, 10108. [\[CrossRef\]](#)
- Uslu, E.; Gavgali, M.; Erdal, M.O.; Yazman, Ş.; Gemi, L. Determination of mechanical properties of polymer matrix composites reinforced with electrospinning N66, PAN, PVA and PVC nanofibers: A comparative study. *Mater. Today Commun.* **2021**, *26*, 101939. [\[CrossRef\]](#)
- Kononova, O.; Krasnikovs, A.; Harjkova, G.; Lusis, V. Numerical simulation of mechanical properties for composite reinforced by knitted fabric. In Proceedings of the International Center for Numerical Methods in Engineering, Barcelona, Spain, 20–25 July 2014; Onate, E., Oliver, X., Huerta, A., Eds.; 2014; pp. 2925–2932.
- Kononova, O.; Krasnikovs, A.; Stonys, R.; Sahmenko, G.; Vitols, R. Investigation of influence of nano-reinforcement on the mechanical properties of composite materials. *J. Civ. Eng. Manag.* **2016**, *22*, 425–433. [\[CrossRef\]](#)
- Ahmadi, Z.; Ravandi, S.A.H.; Haghighat, F.; Dabirian, F. Enhancement of the Mechanical Properties of PAN Nanofiber/Carbon Nanotube Composite Mats Produced via Needleless Electrospinning System. *Fibers Polym.* **2020**, *21*, 1200–1211. [\[CrossRef\]](#)
- Viluma-Gudmona, A.; Lasenko, I.; Sanchaniya, J.V.; Abdelhadi, B. The amber nano fibers development prospects to expand the capabilities of textile 3D printing in the general process of fabrication methods. In *Engineering for Rural Development, Proceedings of the 20th International Scientific Conference, Jelgava, Latvia, 26–28 May 2021*; Latvia University of Life Sciences and Technologies: Jelgava, Latvia; pp. 248–257. [\[CrossRef\]](#)
- Storck, J.L.; Hellert, C.; Brockhagen, B.; Wortmann, M.; Diestelhorst, E.; Frese, N.; Grothe, T.; Ehrmann, A. Metallic Supports Accelerate Carbonization and Improve Morphological Stability of Polyacrylonitrile Nanofibers during Heat Treatment. *Materials* **2021**, *14*, 4686. [\[CrossRef\]](#)
- Vahle, D.; Böttjer, R.; Heyden, K.; Ehrmann, A. Conductive polyacrylonitrile/graphite textile coatings. *AIMS Mater. Sci.* **2018**, *5*, 551–558. [\[CrossRef\]](#)
- Lasenko, I.; Gaidukovs, S.; Rombovska, J. Manufacturing of amber particles suitable for composite fibre melt spinning. *Proc. Latv. Acad. Sci. Sect. B Nat. Exact Appl. Sci.* **2016**, *70*, 51–57. [\[CrossRef\]](#)
- Viluma-Gudmona, A.; Lasenko, I.; Sanchaniya, J.V.; Podgornovs, A. Electro-resistant biotextile development based on fiber reinforcement with nano particles. In Proceedings of the 20th International Scientific Conference Engineering for Rural Development, ERD 2021, Jelgava, Latvia, 26–28 May 2021; pp. 804–812. [\[CrossRef\]](#)
- Sadeghi, S.A.M.; Borhani, S.; Zadhoush, A.; Dinari, M. Single nozzle electrospinning of encapsulated epoxy and mercaptan in PAN for self-healing application. *Polymer* **2020**, *186*, 122007. [\[CrossRef\]](#)

17. Mokhtari-Shourijeh, Z.; Langari, S.; Montazerghaem, L.; Mahmoodi, N.M. Synthesis of porous aminated PAN/PVDF composite nanofibers by electrospinning: Characterization and Direct Red 23 removal. *J. Environ. Chem. Eng.* **2020**, *8*, 103876. [[CrossRef](#)]
18. Janushevskis, A.; Sanchaniya, J.; Vejanand, S. Designing of catamaran hull spine beam. In Proceedings of the 20th International Scientific Conference Engineering for Rural Development, Jelgava, Latvia, 26–28 May 2021; pp. 1685–1691. [[CrossRef](#)]
19. Dehghani, M.; Nadeem, H.; Raghuwanshi, V.S.; Mahdavi, H.; Holl, M.M.B.; Batchelor, W. ZnO/cellulose nanofiber composites for sustainable sunlight-driven dye degradation. *ACS Appl. Nano Mater.* **2020**, *3*, 10284–10295. [[CrossRef](#)]
20. Gaidukovs, S.; Lyashenko, I.; Rombovska, J.; Gaidukova, G. Application of amber filler for production of novel polyamide composite fiber. *Text. Res. J.* **2016**, *86*, 2127–2139. [[CrossRef](#)]
21. Xu, T.-C.; Han, D.-H.; Zhu, Y.-M.; Duan, G.-G.; Liu, K.-M.; Hou, H.-Q. High Strength Electrospun Single Copolyacrylonitrile (coPAN) Nanofibers with Improved Molecular Orientation by Drawing. *Chin. J. Polym. Sci.* **2020**, *39*, 174–180. [[CrossRef](#)]
22. Grauda, D.; Bumbure, L.; Lyashenko, I.; Katashev, A.; Dekhtyar, Y.; Rashal, I. Amber Particles as Living Plant Cell Markers in Flow Cytometry / Dzintara Daļiņas Kā Dzīvu Augu Šūnu Marķieri Plūsmas Citometrijā. *Proc. Latv. Acad. Sci. Sect. B Nat. Exact Appl. Sci.* **2015**, *69*, 77–81. [[CrossRef](#)]
23. Dadvar, S.; Tavanai, H.; Dadvar, H.; Morshed, M.; Ghodsi, F.E. UV-protection and photocatalytic properties of electrospun polyacrylonitrile nanofibrous mats coated with TiO₂ nanofilm via sol-gel. *J. Sol-Gel. Sci. Technol.* **2011**, *59*, 269–275. [[CrossRef](#)]
24. Dubova, I.; Apine, A.; Grauda, D.; Butkauskas, D.; Lasenko, I.; Jankevica, L. Adaptation of methods for the determination of biodegradation of bio-textiles with amber particles. In Proceedings of the International Scientific Conference of the University of Latvia, Innovative and Applied Research in Biology, Riga, Latvia, 5 February 2021; 2021; Volume 3, pp. 269–275. [[CrossRef](#)]
25. Grauda, D.; Miķelsons, A.; Butkauskas, D.; Rašals, D.; Vilcāne, I.; Gobinš, V.; Lasenko, I. Protective properties of biotextile indicated by immature gamete cells flow cytometry and *Drosophila melanogaster* survival tests. In Proceedings of the International Scientific Conference of the University of Latvia, Innovative and applied research in Biology, Riga, Latvia, 5 February 2021; Volume 3, pp. 26–33. [[CrossRef](#)]
26. Wu, M.; Wang, Q.; Li, K.; Wu, Y.; Liu, H. Optimization of stabilization conditions for electrospun polyacrylonitrile nanofibers. *Polym. Degrad. Stab.* **2012**, *97*, 1511–1519. [[CrossRef](#)]
27. Shrestha, R.; Li, P.; Chatterjee, B.; Zheng, T.; Wu, X.; Liu, Z.; Luo, T.; Choi, S.; Hippalgaonkar, K.; de Boer, M.P.; et al. Crystalline polymer nanofibers with ultra-high strength and thermal conductivity. *Nat. Commun.* **2018**, *9*, 1664. [[CrossRef](#)] [[PubMed](#)]
28. Lin, J.; Bang, S.H.; Malakooti, M.H.; Sodano, H.A. Isolation of Aramid Nanofibers for High Strength and Toughness Polymer Nanocomposites. *ACS Appl. Mater. Interfaces* **2017**, *9*, 11167–11175. [[CrossRef](#)] [[PubMed](#)]
29. Zhu, K.; Duan, J.; Guo, J.; Wu, S.; Lu, A.; Zhang, L. High-Strength Films Consisted of Oriented Chitosan Nanofibers for Guiding Cell Growth. *Biomacromolecules* **2017**, *18*, 3904–3912. [[CrossRef](#)] [[PubMed](#)]
30. Yu, L.; Shao, Z.; Xu, L.; Wang, M. High throughput preparation of aligned nanofibers using an improved bubble-electrospinning. *Polymers* **2017**, *9*, 658. [[CrossRef](#)]
31. Guan, Y.; Li, W.; Zhang, Y.; Shi, Z.; Tan, J.; Wang, F.; Wang, Y. Aramid nanofibers and poly (vinyl alcohol) nanocomposites for ideal combination of strength and toughness via hydrogen bonding interactions. *Compos. Sci. Technol.* **2017**, *144*, 193–201. [[CrossRef](#)]
32. Ren, L.; Jiang, Q.; Chen, K.; Chen, Z.; Pan, C.; Jiang, L. Fabrication of a micro-needle array electrode by thermal drawing for bio-signals monitoring. *Sensors* **2016**, *16*, 908. [[CrossRef](#)]
33. Wu, Y.-K.; Wang, L.; Fan, J.; Shou, W.; Liu, Y. A double-switching voltage: Controlling multiple jets in electrospinning. *Mater. Lett.* **2018**, *233*, 359–362. [[CrossRef](#)]
34. Wang, Z.; Sun, B.; Lu, X.; Wang, C.; Su, Z. Molecular Orientation in Individual Electrospun Nanofibers Studied by Polarized AFM-IR. *Macromolecules* **2019**, *52*, 9639–9645. [[CrossRef](#)]
35. Kausar, A. Polyacrylonitrile-based nanocomposite fibers: A review of current developments. *J. Plast. Film Sheeting* **2019**, *35*, 295–316. [[CrossRef](#)]
36. Jeon, I.; Yoon, J.; Kim, U.; Lee, C.; Xiang, R.; Shawky, A.; Xi, J.; Byeon, J.; Lee, H.M.; Choi, M.; et al. High-Performance Solution-Processed Double-Walled Carbon Nanotube Transparent Electrode for Perovskite Solar Cells. *Adv. Energy Mater.* **2019**, *9*, 1901204. [[CrossRef](#)]
37. Rajak, D.K.; Pagar, D.D.; Kumar, R.; Pruncu, C.I. Recent progress of reinforcement materials: A comprehensive overview of composite materials. *J. Mater. Res. Technol.* **2019**, *8*, 6354–6374. [[CrossRef](#)]
38. Barua, B.; Saha, M.C. Investigation on jet stability, fiber diameter, and tensile properties of electrospun polyacrylonitrile nanofibrous yarns. *J. Appl. Polym. Sci.* **2015**, *132*, 41918. [[CrossRef](#)]
39. Jung, J.; Sodano, H.A. Aramid Nanofiber Reinforced Rubber Compounds for the Application of Tire Tread with High Abrasion Resistance and Fuel Saving Efficiency. *ACS Appl. Polym. Mater.* **2020**, *2*, 4874–4884. [[CrossRef](#)]
40. Kaur, N.; Kumar, V.; Dhakate, S.R. Synthesis and characterization of multiwalled CNT—PAN based composite carbon nanofibers via electrospinning. *SpringerPlus* **2016**, *5*, 483. [[CrossRef](#)] [[PubMed](#)]
41. Cai, J.; Chawla, S.; Naraghi, M. Microstructural evolution and mechanics of hot-drawn CNT-reinforced polymeric nanofibers. *Carbon* **2016**, *109*, 813–822. [[CrossRef](#)]
42. Wang, Q.; Yao, Q.; Chang, J.; Chen, L. Enhanced thermoelectric properties of CNT/PANI composite nanofibers by highly orienting the arrangement of polymer chains. *J. Mater. Chem.* **2012**, *22*, 17612–17618. [[CrossRef](#)]

43. Mombini, S.; Mohammadnejad, J.; Bakhshandeh, B.; Narmani, A.; Nourmohammadi, J.; Vahdat, S.; Zirak, S. Chitosan-PVA-CNT nanofibers as electrically conductive scaffolds for cardiovascular tissue engineering. *Int. J. Biol. Macromol.* **2019**, *140*, 278–287. [[CrossRef](#)] [[PubMed](#)]
44. Oberdörster, G.; Castranova, V.; Asgharian, B.; Sayre, P. Inhalation exposure to carbon nanotubes (CNT) and carbon nanofibers (CNF): Methodology and Dosimetry. *J. Toxicol. Environ. Health Part B* **2015**, *18*, 121–212. [[CrossRef](#)]
45. Tan, E.P.S.; Lim, C.T. Physical properties of a single polymeric nanofiber. *Appl. Phys. Lett.* **2004**, *84*, 1603–1605. [[CrossRef](#)]
46. Lim, C.T.; Tan, E.P.S.; Ng, S.Y. Effects of crystalline morphology on the tensile properties of electrospun polymer nanofibers. *Appl. Phys. Lett.* **2008**, *92*, 141908. [[CrossRef](#)]
47. Wong, S.-C.; Baji, A.; Leng, S. Effect of fiber diameter on tensile properties of electrospun poly(ϵ -caprolactone). *Polymer* **2008**, *49*, 4713–4722. [[CrossRef](#)]
48. Arinstein, A.; Burman, M.; Gendelman, O.; Zussman, E. Effect of supramolecular structure on polymer nanofibre elasticity. *Nat. Nanotechnol.* **2007**, *2*, 59–62. [[CrossRef](#)] [[PubMed](#)]
49. Pai, C.-L.; Boyce, M.C.; Rutledge, G.C. Mechanical properties of individual electrospun PA 6(3)T fibers and their variation with fiber diameter. *Polymer* **2011**, *52*, 2295–2301. [[CrossRef](#)]
50. Chew, S.Y.; Hufnagel, T.C.; Lim, C.T.; Leong, K.W. Mechanical properties of single electrospun drug-encapsulated nanofibres. *Nanotechnology* **2006**, *17*, 3880–3891. [[CrossRef](#)]
51. Shin, M.K.; Kim, S.I.; Kim, S.J.; Kim, S.-K.; Lee, H.; Spinks, G.M. Size-dependent elastic modulus of single electroactive polymer nanofibers. *Appl. Phys. Lett.* **2006**, *89*, 231929. [[CrossRef](#)]
52. Naraghi, M.; Arshad, S.N.; Chasiotis, I. Molecular orientation and mechanical property size effects in electrospun polyacrylonitrile nanofibers. *Polymer* **2011**, *52*, 1612–1618. [[CrossRef](#)]
53. Qanati, M.V.; Rasooli, A.; Rezvani, M. Main structural and mechanical properties of electrospun PAN-based carbon nanofibers as a function of carbonization maximum temperature. *Polym. Bull.* **2022**, *79*, 331–355. [[CrossRef](#)]
54. Yang, H.; Fan, F.R.; Xi, Y.; Wu, W. Bio-Derived Natural Materials Based Triboelectric Devices for Self-Powered Ubiquitous Wearable and Implantable Intelligent Devices. *Adv. Sustain. Syst.* **2020**, *4*, 2000108. [[CrossRef](#)]